

Drag force and reconfiguration of cultivated *Saccharina latissima* in current

Jiarui Lei^{a*}, Dixia Fan^b, Andrea Angera^c, Yuming Liu^b, Heidi Nepf^a

^a Department of Civil and Environmental Engineering, MIT, Cambridge, MA 02138

^b Department of Mechanical Engineering, MIT, Cambridge, MA 02138

^c Springtide Seaweed, LLC, Gouldsboro, ME 04607

Abstract

The design of aquaculture systems requires an understanding of the drag forces on cultivated kelp. This study measured the drag on line segments of cultivated *Saccharina latissima* in a tow tank. The drag on segments of farm line with full plants and with stipes alone (fronds removed) was measured at tow speeds of 0.10 to 0.50 m/s. The drag on individual fronds cut from the line was also measured. Video images were collected to evaluate the plant reconfiguration. Both kelp blades and stipes contributed to the total drag force on the line bundle. Within the velocity range of our experiments, the kelp blades were essentially horizontal. However, the pronation of kelp stipes increased as flow velocity increased. The reconfiguration of kelp stipes was observed to decrease the vertical extent of the kelp bundle. Due to this reconfiguration, the measured force, F , increased with velocity, U , at a rate slower than quadratic, and was consistent with scaling laws derived for reconfiguration. Specifically, $F \sim U^\alpha$ with $\alpha = 1.35 \pm 0.17$.

Keywords: Aquaculture, Kelp, Reconfiguration, Drag force, Flow-vegetation interaction

*Corresponding author.

Email: garylei@mit.edu; Jiarui_lei@uml.edu

1. Introduction

Kelp provides many ecosystem services, such as providing food and shelter areas for a variety of animals (Costanza et al. 1997). Kelp can also sequester carbon dioxide and recycle nutrients (Duarte et al. 2017, Xiao et al. 2017). Both natural kelp forests and kelp aquaculture can significantly influence local hydrodynamics by attenuating currents and waves (Gaylord et al. 2007, Rosman et al. 2007, Dubi and Torum, 1994, Plew et al. 2005). Jackson and Winant (1983) found that a kelp forest (*Macrocystis pyrifera*) attenuated current by up to 80%. Rosman et al. (2007) observed that current reduction within a kelp forest was higher during seasons with greater surface canopy coverage, with the reduction of current ranging from 50% to 80%. Unlike natural kelp forests that grow from the seafloor, kelp farms are suspended or floating canopies. Because of the higher concentration of blades near the surface, the attenuation of currents and waves by kelp farms may be more significant than that by natural kelp forests. For example, Zhu and Zou (2017) note that canopies suspended near the surface attenuate more wave energy than canopies at the seafloor, because wave energy is higher near the surface and decreases toward the bed. The reduction of waves and current are directly related to the hydrodynamic drag associated with the kelp.

Hydrodynamic drag is also a key design parameter for kelp farms. To maximize yield per cost, kelp farm lines are densely seeded, which results in high drag on the lines. An accurate estimation of kelp line drag is essential for the design of safe mooring systems in aquaculture kelp farming. A handful of previous studies has investigated the hydrodynamic characteristics of cultivated kelp under unidirectional flow. Buck and Buchholz (2005) found that the drag force on a bundle of wild kelp blades is two to five times greater than that on cultivated kelp of similar blade area. Vettori and Nikora (2019) measured drag on individual blades of *Saccharina latissima* and observed that after exposure to a high current, the blade drag force declined over several minutes due to a compression of blade's ruffled edge, i.e., due to a reconfiguration of the blade shape. Endresen et al (2019) observed that the drag on a line segment of cultivated kelp increased with velocity, but at a rate that was weaker the expected quadratic dependence of a rigid body. This may be explained by reconfiguration at the blade scale (as noted by Vettori and Nikora, 2019) or at the scale of the kelp bundle, which is explored in this study.

The objective of this study was to explore how the drag on a line of cultivated kelp varied with velocity and to explore the connection to bundle-scale reconfiguration. A series of experiments were conducted to measure the drag on the full kelp-stipe-line bundle, on the stipes alone and on individual blades. The reconfiguration of kelp stipes and blades was measured with digital imaging and used to interpret the dependence of drag force on current speed. A review of the scaling laws for the drag force on and the reconfiguration of flexible vegetation is provided in section 2.

2. Reconfiguration

Blades and stipes bend in response to unidirectional current. This reconfiguration can be described by two dimensionless parameters (e.g., Luhar and Nepf 2011). The Cauchy number, Ca , is the

ratio of hydrodynamic drag to the restoring force due to the rigidity. The buoyancy parameter, B , is the ratio between buoyancy and the restoring force due to the rigidity.

$$Ca = \frac{\frac{1}{2}C_D\rho bU^2l^3}{EI}. \quad (1)$$

$$B = \frac{\Delta\rho g b d l^3}{EI}. \quad (2)$$

For simplicity, we explore these parameters in the context of a generic flat blade held perpendicular to the flow at its mid-point (Figure 1). The blade has thickness d , width b , and length l . C_D is the drag coefficient, ρ is the density of water, $\Delta\rho$ is the difference in density between the water and the blade, U is the current speed, E is the modulus of elasticity, and I is the bending moment of inertia, which for a flat blade, $I = \frac{1}{12}bd^3$.

In previous studies (Luhar and Nepf 2011), the effective length, l_e , was introduced to characterize the impact of reconfiguration on the drag force on a single blade. The effective length is defined as the length of a rigid blade that experiences the same drag force as a flexible blade of length l . By definition, the hydrodynamic drag acts over length-scale l_e , such that the force can be written $F = \frac{1}{2}C_D\rho b l_e U^2$. Balancing this with the restoring force due to rigidity $\frac{EI}{l_e^2}$ yields the following scaling law for objects that reconfigure in a single direction, called 2D reconfiguration (Alben et al. 2002, Gosselin et al 2010).

$$\frac{l_e}{l} \sim Ca^{-1/3} \quad (3)$$

Luhar and Nepf (2011) further considered the buoyancy parameter, and provided a formula to predict $\frac{l_e}{l}$ as a function of Ca and B . However, for *Saccharina latissima*, used in this study, the blades are close to neutrally buoyant, such that buoyancy did not significantly impact the blade posture in the water (Vettori and Nikora 2017). In this case, Eqn. 16 in Luhar and Nepf (2011) simplifies to Eqn 3. Note that the effective length reflects, l_e , reflects the reduction in drag associated with both the reduction in frontal area (h in Figure 1) and the tendency toward a more streamlined shape. Because the streamlining is dynamically important, $h > l_e$, and h follows a weaker dependence with Ca . Specifically, (eqn. 4 and Fig. 2 in Luhar and Nepf 2013 with $B = 0$).

$$\frac{h}{l} \sim Ca^{-1/4} \sim U^{-1/2} \quad (4)$$

In this study, we explored whether the bundle of kelp stipes and blades responds to flow in a manner similar to 2D reconfiguration. For 2D reconfiguration of the kelp bundle, h will decrease with increasing velocity following Eqn 4., and the drag force per line length (L) will follow

$$\frac{F}{L} = \frac{1}{2} C_D \rho b l_e U^2 \sim \frac{1}{2} C_D \rho b (l Ca^{-\frac{1}{3}}) U^2 \sim (U^{-2/3} U^2) \sim U^{4/3} \quad (5)$$

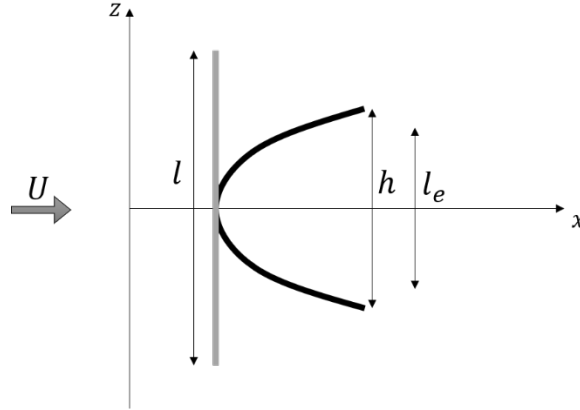


Figure 1. A flat blade of length l (grey line) is held perpendicular to the flow U . For $Ca > 1$, the blade reconfigures to the shape shown with black line. The reconfigured blade has smaller dimension (h) and is also a more streamlined shape, both of which combine to produce an effective length l_e , which is the length of rigid blade producing the same drag. The blade shown is pinned at the center, similar to the configuration considered by Alben et al 2002, and Gosselin et al 2010). This reconfigured blade is geometrically similar to a stipe-blade bundle. Luhar and Nepf (2011) considered a blade of length $l/2$ pinned at the bed, which, from symmetry, produces the same scaling laws.

3 Materials and Methods

3.1 Kelp sample

Kelp samples were collected from Springtide Seaweed Lease FREN PI4, Sorrento, Maine (Lat/Lon: 68.177291, 44.458834). Two sections of line (79 cm and 102 cm in length) containing cultivated *S. Latissima* were extracted from the longlines at 7:30 am on July 16th, 2020. The kelp was stored in a cooler with bagged ice to maintain temperature and transported to the MIT Towing Tank laboratory within 6 hours of collection. The narrower bundle was used for force measurements on the same day, and the wider one was tested the day after (July 17th, 2020). Each kelp bundle consisted of hundreds of kelp plants, each consisting of the holdfast, the stipe, and a single blade. The number of fronds were counted for each bundle. The length and width of 75 randomly selected blades were measured.



Figure 2. The 40 in-wide kelp bundle tested on July 17th, 2020. The kelp fronds, including the stipe and the blade, have a maximum length of 1.8 m.

3.2 Force measurement and visualization

The force measurements and visualization were conducted in the MIT Towing Tank, which consists of a 30-m testing tank that is 2.5 m in width and 1.2 m in depth. The towing tank facilities have been used to test hydrodynamics and structural response of various underwater flexible structure (Fan, et al. 2019). Two photos of the kelp bundle under water during a tow are also shown in Figure 3. So that the drag force did not exceed the capacity of the load cell, each bundle was split into two segments (listed as Line Length in Table 1). Each line segment was tied to a horizontal bar (holder) using thin nylon rope, and the bar was attached to a load cell (Figure 3a). The drag force was measured at 1000 Hz at towing speeds from 0.10 to 0.50 m/s. A low-pass filter was used to remove high-frequency noise. The filtered force was used to estimate the time-mean, F_{total} and standard deviation σ_{total} of the force time series. The time mean and SD force on the holder was also measured at each tow speed, F_{holder} and σ_{holder} . The drag on the kelp bundle was calculated as

$$F = F_{total} - F_{holder} \quad (6)$$

The uncertainty in F was calculated as the standard deviation of F_{total} , as the standard deviation in F_{holder} was negligible compared to that of F_{total} . Drag was also measured for a bundle of kelp stipes by cutting off the blades (Case 6). The force on five longest blades from the 56-cm bundle was also measured (Case 8).

Table 1. Experimental cases. Case 1 measured the holder alone. Cases 2, 3, 4, 5, and 7 measured lines with stipe and blades. Case 6 measured line with stipes only. Case 8 measured the five longest blades extracted from the 56-cm line. Case 9 measured the 56-cm line with the five longest blades removed. The exponent α in the fitted drag law $F \sim U^\alpha$ and the exponent β in the bundle length-scale, $h \sim U^\beta$

Case	Source	Form	Line length	No. of fronds	Towing speed	Fitted α	Fitted β
1	Holder	N/A	N/A	N/A	0.10 to 0.50 m/s	2.00	N/A
2	79-cm bundle	Kelp bundle	46 cm	N/A	0.10 to 0.40 m/s	1.20	-0.31
3	79-cm bundle	Kelp bundle	33 cm	240±10	0.10 to 0.50 m/s	1.36	-0.23
4	102-cm bundle	Kelp bundle	102 cm	660±20	0.10 to 0.25 m/s	1.31	N/A
5	102-cm bundle	Kelp bundle	46 cm	280±10	0.10 to 0.40 m/s	1.48	-0.35
6	102-cm bundle	Stipes only	46 cm	280±10 (stipes)	0.10 to 0.40 m/s	1.86	N/A
7	102-cm bundle	Kelp bundle	56 cm	380±10	0.10 to 0.40 m/s	1.33	-0.30
8	102-cm bundle	Blades only	N/A	5	0.10 to 0.40 m/s	1.35	N/A
9	102-cm bundle	Kelp bundle	56 cm	375±10	0.10 to 0.40 m/s	1.23	N/A

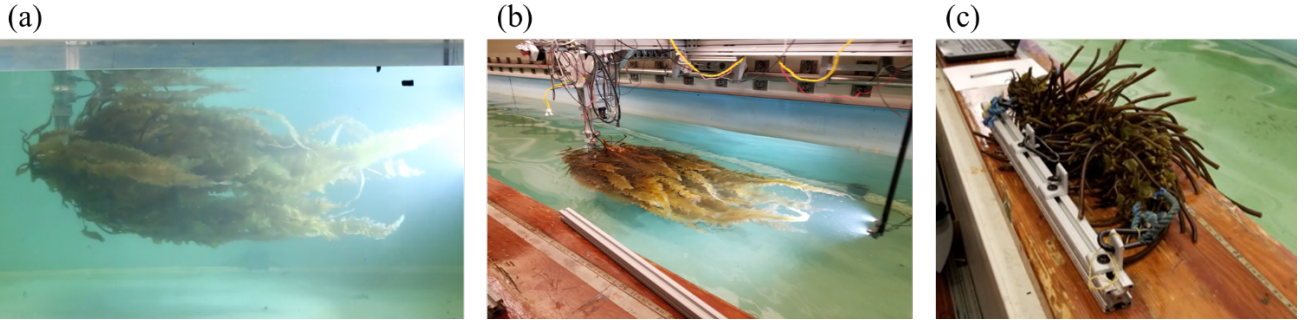


Figure 3. A kelp bundle attached to horizontal holder and towed underwater. (a) side view. (b) top view (c) stipes only (case 6).

The kelp bundle was recorded by a Canon 5D Mark III camera at 50 frames per second throughout the towing process. Images were extracted to measure the vertical length-scale of the bundle, h , shown with black line in Figure 4. The upper and the lower red lines in Figure 4 indicate the water surface and the bed at the centerline of the kelp bundle, respectively. Note that the wide-angle lens distorts the image. To compensate the impact of distortion on the location of the water surface and the bed, we determined the water surface (upper red lines in Figure 4(a)(b)) based on the reflection of the kelp and the holder. Also, the bed (lower red lines in Figure 4(a)(b)) was the centerline of the shadow of the kelp. For consistency, length-scale h was always measured at a fix distance from the holder (45 cm, indicated by the short red line). Figure 4 (a)(b) compare the kelp-stipe bundle at the lowest and highest tow speed. Figure 4 (c)(d) compare the individual blades at the lowest and highest tow speed.

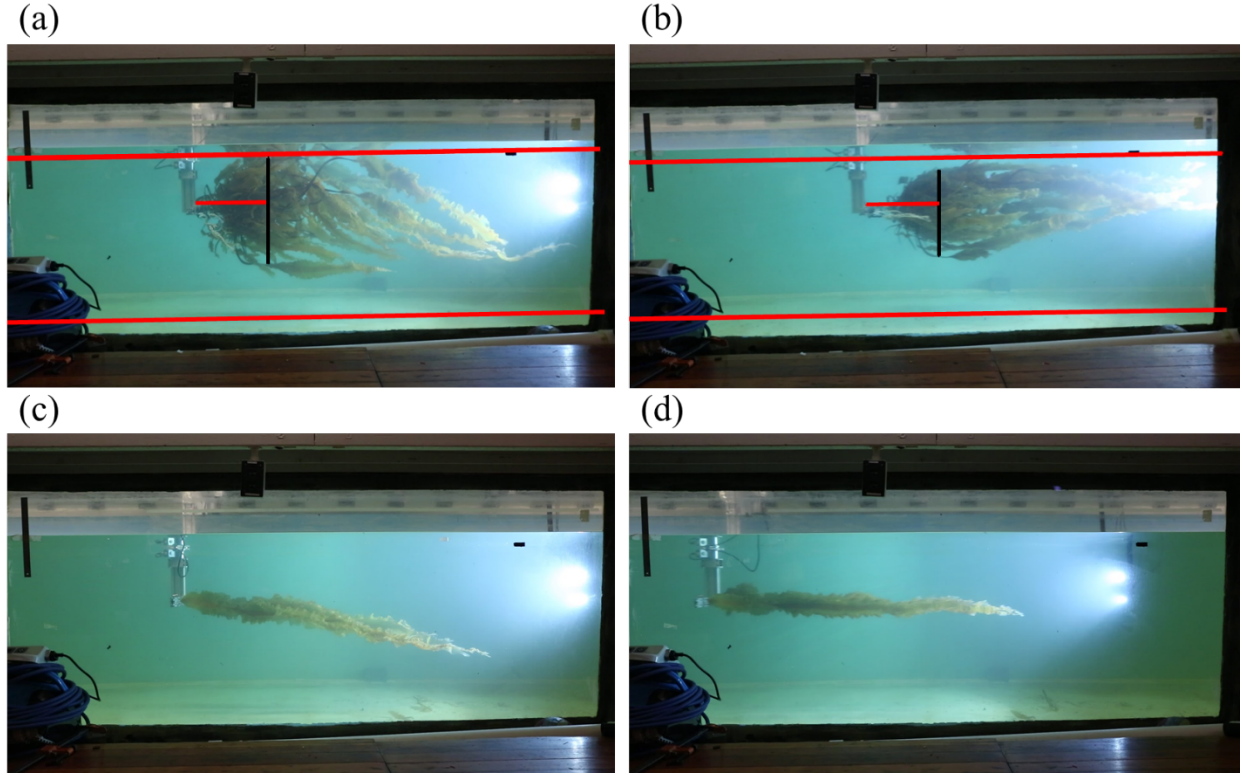


Figure 4. Image of Case 5 stipe-blade bundles at (a) $U = 0.10$ m/s and (b) $U = 0.40$ m/s. Images from Case 8 with five individual blades at (c) $U = 0.10$ m/s and (d) $U = 0.40$ m/s.

4 Results

4.1 Drag per line length

For each of the line segments (Cases 2 ,3 ,4 ,5 and 7), the drag force per line length (F/L) increased with tow velocity, but with a dependence that was weaker than quadratic (Figure 5). Specifically, in each case $F/L \sim U^\alpha$, with $\alpha = 1.34 \pm 0.12$, based on the average across the full kelp bundle cases (Table 1). The uncertainty in α reflects both the average uncertainty in each fit ($= 5\%$ based on 95% CI) and the variation among cases ($= 8\%$). This dependence was consistent with 2D reconfiguration, for which $\alpha = 4/3$ (Eqn. 5). Note that the drag per line length does not vary systematically with line length. For example, the maximum (red) and minimum (blue) drag were both observed for a line length of 18 inches, and the longest line (40 inches) fell in between them. This suggests that the lines were long enough to resemble 2-D conditions, i.e. representative of an infinitely long line. The range in magnitude of F/L likely reflects differences in the number and maturity (length) of blade per line length. For example, Endresen et al (2019) considered lines of sugar kelp with fewer fronds per length (see Figure 5 in Endresen et al. 2019), and measured a lower range of drag, reaching 25 N/m at a tow speed of 0.4 m/s, compared to 20 to 80 N/m in this study. Importantly, Endresen et al (2019) observed a similar velocity dependence, with $\alpha = 1.43 \pm 0.11$ (SD), based on Table 3 in their paper.

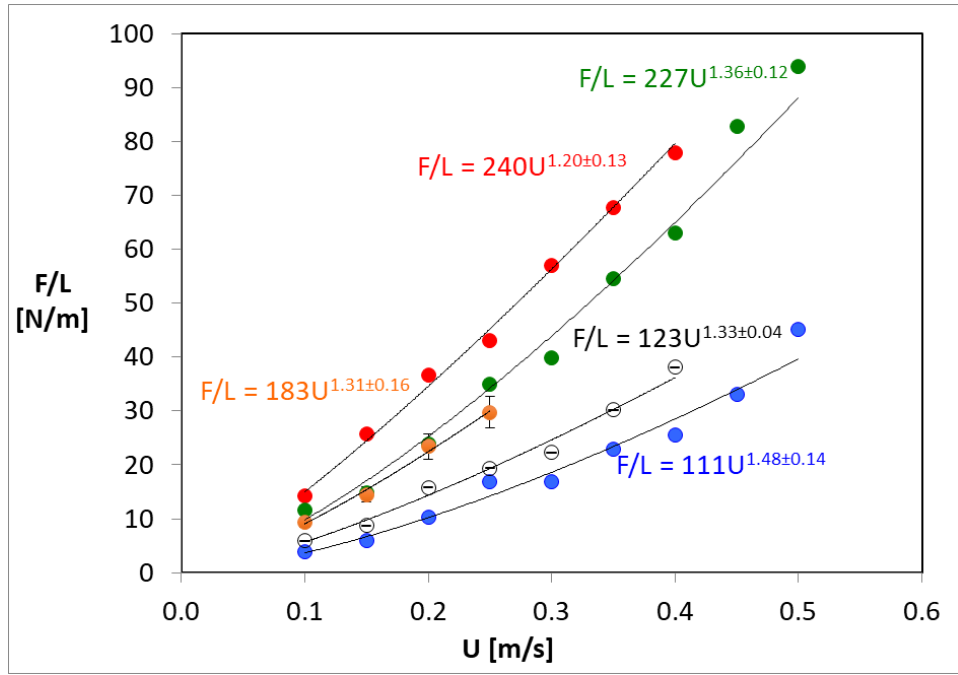


Figure 5. Drag force per line length for each kelp bundle as a function of tow speed. Red markers denote Case 2 (Day 1, 46 cm bundle). Green markers denote Case 3 (Day 1, 33 cm bundle). Orange markers denote Case 4 (Day 2, 102 cm bundle). Blue markers denote Case 5 (Day 2, 46 cm bundle). White markers denote Case 7 (Day 2, 56 cm bundle). The fitted equation for each case is shown on the plot.

4.2 Drag on individual kelp blades

The five longest blades from the 56 cm bundle were separated from the bundle and evenly distributed across the mounting bar (Figure 3 (c) and 3 (d)). Under all flow conditions, the blades were close to horizontal. Specifically, the maximum angle with respect to horizontal direction was 10 degree, at the lowest tow speed, $U = 0.10$ m/s. Although the kelp blades remained nearly horizontal, the drag force did not follow the quadratic dependence expected for a flat plate. The total drag force on the five blades increased with tow speed, but at a rate that was weaker than quadratic (Figure 6). Specifically, $F \sim U^\alpha$, with $\alpha = 1.35 \pm 0.10$ (95 % CI). This was consistent with the drag on individual blades measured by Vettori and Nikora (2019) for the same species (*S. latissima*). Specifically, they found $\alpha = 1.4$ to 1.8. They attributed the diminished velocity dependence ($\alpha < 2$) to the reconfiguration of the compression of the ruffles along the edges the blades.

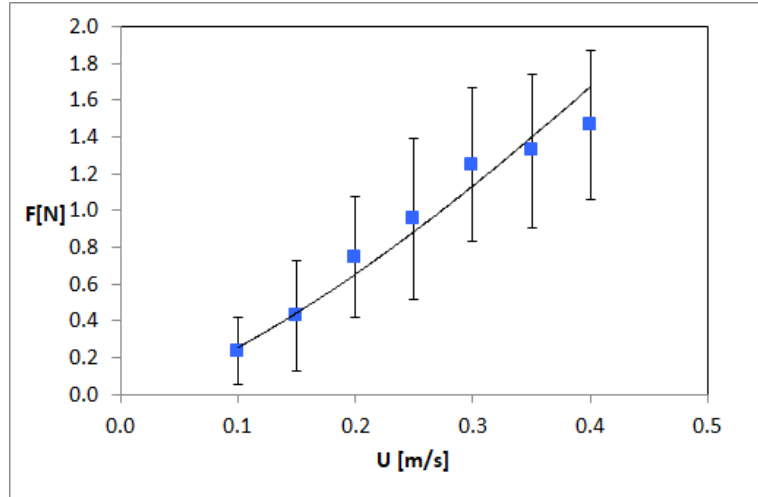


Figure 6. Drag force versus tow velocity for the five longest blades (Case 8). The curve denotes a power-fit, which yielded $\alpha = 1.35 \pm 0.10$ (95 % CI). Vertical bars denote standard deviation in measured force.

4.3 Drag on bundle of stipes without blades

All blades were cut off the 46-cm line segment, leaving only the stipes (Case 6). The force on the stipe bundle exhibited a nearly quadratic relationship with tow speed. Specifically, $F \sim U^\alpha$, with $\alpha = 1.86 \pm 0.06$ (95% CI, Table 1). The quadratic dependence indicated that the stipes were effectively rigid, i.e., did not reconfigure significantly due to the drag generated by the stipe alone. However, when the blades were attached, their drag acted on the stipes, resulting in the reconfiguration of the bundle, discussed in the next section.

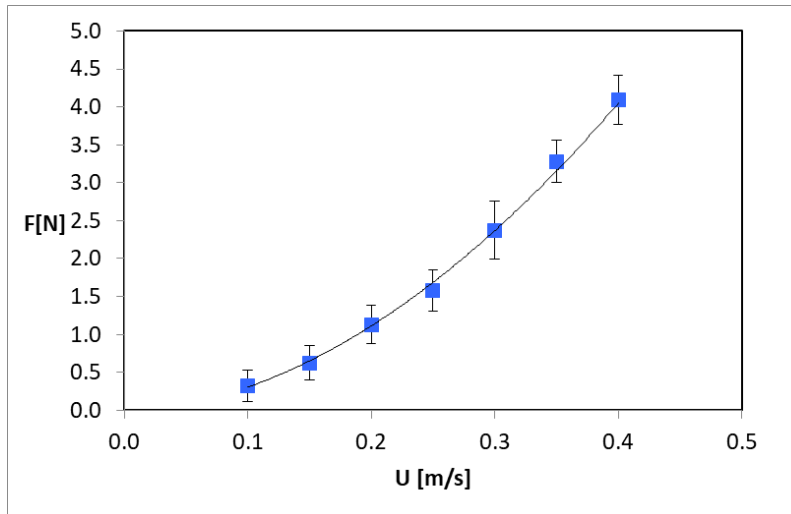


Figure 7. Drag force versus tow velocity for Case 6, the 46-cm line segment with blades cut away, leaving just the stipes. The black curve denotes the power-fit. Vertical bars denote the standard deviation of the measured drag force.

4.4 Reconfiguration of the kelp bundle

The vertical extent of the kelp bundle, h , decreased with increasing tow velocity, U (Figure 8). Specifically, $h \sim U^\beta$, with $\beta = -0.31, -0.23, -0.35$, and -0.30 for Case 2, 3, 5, and 7, respectively. Averaging across all cases $\beta = -0.3 \pm 0.1$, with the uncertainty reflecting both the fitting uncertainty (11% based on 95% CI) and the variation between line segments (17 %). The exponent was a bit smaller than that expected to 2D reconfiguration ($\beta = -0.5$, Eqn. 4), which may be attributed to the more complex geometry of multiple bending elements, compared to the single element (Figure 1) upon which the scaling was based. In addition, for the single element (Figure 1), the drag was distributed evenly along the element. However, for the stipes, a significant portion of the drag came from tension communicated from the blades, i.e. the drag distribution on the stipe was different.

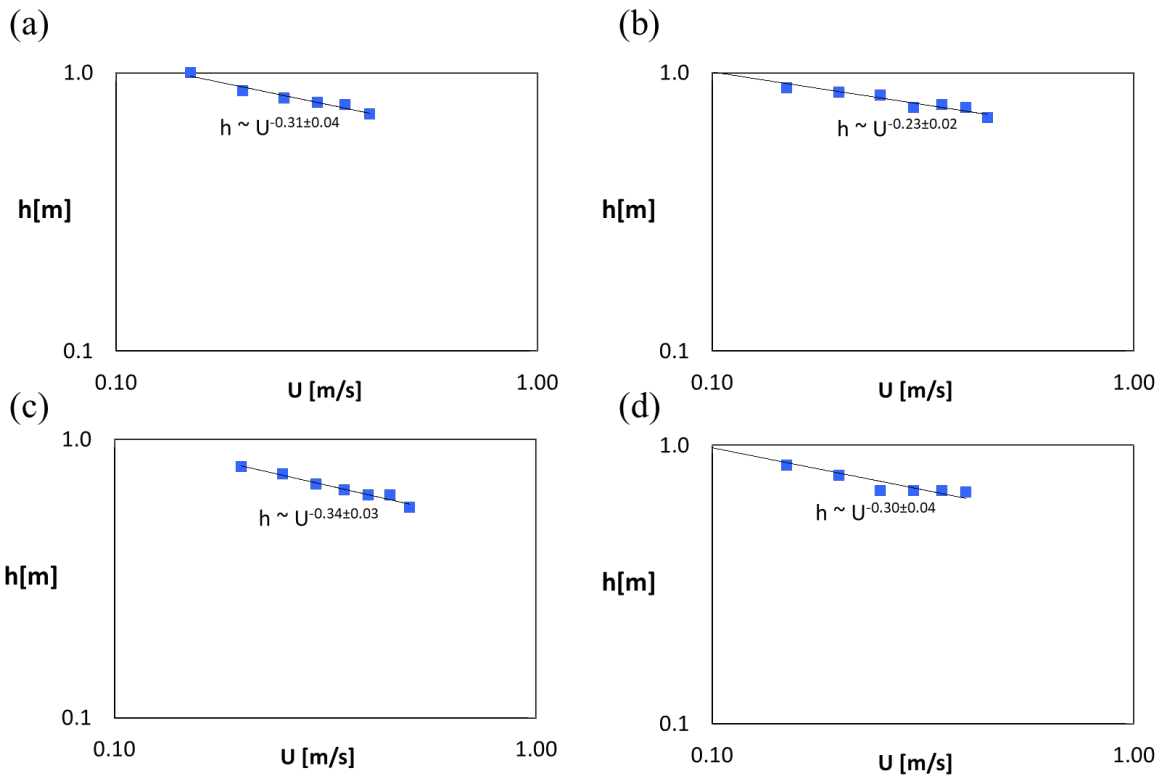


Figure 7. Height of kelp bundle, h , versus tow speed, U . (a) Case 2, 46-cm line segment (Day 1). (b) Case 3, 33-cm line segment (Day 1). (c) Case 5, 46-cm line-segment (Day 2). (d) Case 7, 56-cm line segment (Day 2). Note that the exponent variation was not correlated with the test day, indicating that the kelp material properties did not change significantly between test Day 1 and 2.

5 Discussion

5.1 Impact of reconfiguration on drag force

The vertical extent of the kelp bundle decreased with increasing tow speed, $h \sim U^{-0.30 \pm 0.10}$. Since the kelp blades remained nearly horizontal under all flow conditions, h defined the frontal area per length of cultivated line, determining the drag on the line. The change in kelp frontal area was attributed to the bending of stipes that decreased h and led to a more streamlined stipe distribution. It is interesting to note that the reconfiguration of stipes was not observed when the blades were removed (section 4.2) and that drag from the blades was required to bend the stipes.

Similarly, Zhang and Nepf (2020) showed that drag on the leaves of a freshwater plant determined the reconfiguration of the central stem. In short, the reconfiguration of the stipe bundle was clearly observed, with a velocity dependence close to that expected for 2D reconfiguration (Eqn. 4), which suggested that the observed dependence of drag on velocity can also be explained by 2D reconfiguration of the kelp bundle (Eqn. 3). As an additional point, the drag on individual blades had dependence $F \sim U^{1.35 \pm 0.10}$ (section 4.2), and this dependence was attributed to reconfiguration of the ruffles, previously suggested by Vettori and Nikora (2019), who studied individual blades of the same species (*S. latissima*). This dependence was similar that observed for the full bundle, so that the relative impact of blade-scale and bundle-scale reconfiguration could not be separated.

5.2 Extension to real kelp farms

As discussed in section 4.1, the drag per line length observed in the tow tank was representative of 2D conditions, and thus can be directly applied to real kelp farms with line lengths much longer than those tested in the tow tank. Combining the five cases present in Figure 5, the average drag force per line length was

$$\frac{F}{L} \left[\frac{N}{m} \right] = (180 \pm 60) U^{(1.35 \pm 0.17)} \quad (7)$$

with the uncertainty reflecting both the fitting uncertainty (based on 95% CI) and the variation between different cases. Other studies have observed similar drag dependence. Similar to this study, Endresen et al. (2019) measured drag on line segments of cultivated *S. latissima*. They had four line segments spanning 51 to 205 plants per meter of line, which was smaller than the density in this study (600 to 700 plants per meter, from Table 1). Using Table 3 in Endresen et al (2019) to calculate the average of the four segments $\frac{F}{L} = (62 \pm 9) U^{(1.43 \pm 0.11)}$, with uncertainty estimated as SD . The smaller prefactor reflected the smaller number of fronds per line length. Note that the velocity dependence in both Endresen and the present study agreed within uncertainty, indicating the same reconfiguration mechanism. However, the prefactor differed, due to differences in the number of blades per line length. More studies are needed to better describe how the prefactor varies with kelp maturity and seeding density.

6 Conclusion

Drag force on and reconfiguration of dense aggregates of cultivated kelp were measured in a tow tank. The height of the stipe region decreased with increasing tow speed, and the velocity dependence was consistent with 2D reconfiguration of the stipe bundle. Further, the drag increased with velocity at a rate smaller than quadratic, $F \sim U^{1.35 \pm 0.17}$, which was also consistent with 2D reconfiguration. Comparison to a similar study with cultivated lines of a smaller density showed a similar velocity dependence, indicating that the reconfiguration mechanism was not dependent on line density (fronds / m). However, the total force was dependent on line density, indicating that drag laws must account for the kelp maturity and seeding density on the line.

Acknowledgements

This work was supported by NOAA-NSG Exploring New Aquaculture Opportunities.

All data are included in this manuscript.

References

- [1] Alben, S., M. Shelley, and J. Zhang (2002). Drag reduction through self-similar bending of a flexible body. *Nature*, 420(6915), 479, doi: 10.1038/nature01232.
- [2] Buck, B.H. and Buchholz, C.M., 2005. Response of offshore cultivated *Laminaria saccharina* to hydrodynamic forcing in the North Sea. *Aquaculture*, 250(3-4), pp.674-691, doi: 10.1016/j.aquaculture.2005.04.062.
- [3] Costanza, R., R. d'Arge, R. De Groot, S. Farber, M. Grasso, B. Hannon, K. Limburg, S. Naeem, R. V. O'Neill, J. Paruelo, and R. G. Raskin (1997). The value of the world's ecosystem services and natural capital. *Nature*, 387(6630), 253-260, doi: 10.1038/387253a0.
- [4] Duarte, C.M., Wu, J., Xiao, X., Bruhn, A. and Krause-Jensen, D., 2017. Can seaweed farming play a role in climate change mitigation and adaptation? *Frontiers in Marine Science*, 4, p.100, doi: 10.3389/fmars.2017.00100.
- [5] Dubi, A. and Tørum, A., 1995. Wave damping by kelp vegetation. In *Coastal Engineering 1994* (pp. 142-156), doi: 10.1061/9780784400890.012.
- [6] Endresen, P.C., Norvik, C., Kristiansen, D., Birkevold, J. and Volent, Z., 2019, June. Current Induced Drag Forces on Cultivated Sugar Kelp. In *International Conference on Offshore Mechanics and Arctic Engineering* (Vol. 58837, p. V006T05A007). American Society of Mechanical Engineers, doi: 10.1115/OMAE2019-96375.
- [7] Fan, D., Wang, Z., Triantafyllou, M. S., and Karniadakis, G. E., 2019. Mapping the properties of the vortex-induced vibrations of flexible cylinders in uniform oncoming flow. *Journal of Fluid Mechanics*, 881, 815-858, doi: 10.1017/jfm.2019.738
- [8] Fredriksson, D.W., Dewhurst, T., Drach, A., Beaver, W., Gelais, A.T.S., Johndrow, K. and Costa-Pierce, B.A., 2020. Hydrodynamic Characteristics of a Full Scale Kelp Model for Aquaculture Applications. *Aquacultural Engineering*, p.102086, doi: 10.1016/j.aquaeng.2020.102086.

- [9] Gaylord, B., Rosman, J.H., Reed, D.C., Koseff, J.R., Fram, J., MacIntyre, S., Arkema, K., McDonald, C., Brzezinski, M.A., Largier, J.L. and Monismith, S.G., 2007. Spatial patterns of flow and their modification within and around a giant kelp forest. *Limnology and Oceanography*, 52(5), pp.1838-1852, doi: 10.4319/lo.2007.52.5.1838.
- [10] Gosselin, F., De Langre, E. and Machado-Almeida, B., 2010. Drag reduction of flexible plates by reconfiguration, doi: 10.1017/s0022112009993673.
- [11] Jackson, G.A. and Winant, C.D., 1983. Effect of a kelp forest on coastal currents. *Continental Shelf Research*, 2(1), pp.75-80, doi: 10.1016/0278-4343(83)90023-7.
- [12] Lei, J. and Nepf, H., 2019. Blade dynamics in combined waves and current. *Journal of Fluids and Structures*, 87, pp.137-149, doi: 10.1016/j.jfluidstructs.2019.03.020.
- [13] Luhar, M., and H. Nepf (2011) Flow induced reconfiguration of buoyant and flexible aquatic vegetation. *Limnol. Ocean.*, 56(6):2003-2017, doi:10.4319/lo.2011.56.6.2003.
- [14] Luhar, M. and Nepf, H.M., 2013. From the blade scale to the reach scale: A characterization of aquatic vegetative drag. *Advances in Water Resources*, 51, pp.305-316, doi: 10.1016/j.advwatres.2012.02.002.
- [15] Luhar, M. and H. Nepf (2016) Wave-induced dynamics of flexible blades. *J. Fluids & Structures*, 61:20-41, doi.org/10.1016/j.jfluidstructs.2015.11.007.
- [16] Plew, D.R., Stevens, C.L., Spigel, R.H. and Hartstein, N.D., 2005. Hydrodynamic implications of large offshore mussel farms. *IEEE Journal of Oceanic Engineering*, 30(1), pp.95-108, doi: 10.1109/JOE.2004.841387.
- [17] Rosman, J.H., Koseff, J.R., Monismith, S.G. and Grover, J., 2007. A field investigation into the effects of a kelp forest (*Macrocystis pyrifera*) on coastal hydrodynamics and transport. *Journal of Geophysical Research: Oceans*, 112(C2), doi: 10.1029/2005JC003430.
- [18] Xiao, X., Agusti, S., Lin, F., Li, K., Pan, Y., Yu, Y., Zheng, Y., Wu, J. and Duarte, C.M., 2017. Nutrient removal from Chinese coastal waters by large-scale seaweed aquaculture. *Scientific reports*, 7, p.46613, doi: 10.1038/srep46613.
- [19] Vettori, D. and Nikora, V., 2017. Morphological and mechanical properties of blades of *Saccharina latissima*. *Estuarine, Coastal and Shelf Science*, 196, pp.1-9, doi: 10.1016/j.ecss.2017.06.033.
- [20] Vettori, D. and Nikora, V., 2019. Flow-seaweed interactions of *Saccharina latissima* at a blade scale: turbulence, drag force, and blade dynamics. *Aquatic Sciences*, 81(4), p.61, doi: 10.1007/s00027-019-0656-x.
- [21] Vettori, D. and Nikora, V., 2020. Hydrodynamic performance of vegetation surrogates in hydraulic studies: a comparative analysis of seaweed blades and their physical models. *Journal of Hydraulic Research*, 58(2), pp.248-261, doi: 10.1080/00221686.2018.1562999.
- [22] XU, M. and KOMATSU, T., 2016. Field measurements of drag force on *Sargassum horneri* (Turner) C. Agardh towed by a boat and estimation of drag coefficient. *La mer*, 54, pp.77-86.
- [23] Zhu, L. and Zou, Q., 2017. Three-layer analytical solution for wave attenuation by suspended and non-suspended vegetation canopy. *Coastal Engineering Proceedings*, 1(35), p.27, doi: 10.9753/icce.v35.waves.27.